# Fluctuations in export productivity over the last century from sediments of a southern Chilean fjord (44°S)

Julio Sepúlveda[1,2*], Silvio Pantoja[2,3], Konrad Hughen[4], Carina Lange[2,3], Fidelina Gonzalez[5], Práxedes Muñoz[6], Lorena Rebolledo[1,2], Rodrigo Castro[2], Sergio Contreras[1,2], Alejandro Ávila[2], Pamela Rossel[1,2], Gisella Lorca[1,2], Marco Salamanca[3] and Nelson Silva[7]

[1]Graduate Program in Oceanography, Department of Oceanography, University of Concepción, P.O. Box 160-C, Concepción, Chile

[2]Center for Oceanographic Research in the eastern South Pacific (FONDAP-COPAS), University of Concepción, P.O. Box 160-C, Concepción, Chile

[3]Department of Oceanography, School of Natural Sciences and Oceanography, University of Concepción, P.O. Box 160-C, Concepción, Chile

[4]Department of Marine Chemistry and Geochemistry, Woods Hole Oceanographic Institution, Woods Hole, MA 02543, USA

[5]Department of Molecular Biology, School of Biological Sciences, University of Concepción, P.O. Box 160-C, Concepción, Chile

[6]Department of Marine Biology, North Catholic University, Campus Guayacán, P.O. Box 117, Coquimbo, Chile

[7]School of Marine Sciences, Catholic University of Valparaiso, Av. Altamirano 1480, Valparaiso, Chile

*Corresponding author. Present address: International Graduate Program – Proxies in Earth History (EUROPROX). Research Center of Ocean Margins (RCOM), University of Bremen, Leobener Strasse, MARUM, D-28359 Bremen, Germany.

E-mail address: sepulved@uni-bremen.de (J. Sepúlveda)

Tel: + (49) (421) 218-65742; fax: + (49) (421) 218-65715

KEYWORDS: Paleoproductivity, organic matter, fjords, Chile.

**Abstract**

Here we present the first reconstruction of changes in surface primary production during the last century from the Puyuhuapi fjord in southern Chile, using a variety of parameters (diatoms, biogenic silica, total organic carbon, chlorins, and proteins) as productivity proxies. Two sediment cores from the head and the center of the fjord were analyzed and compared to gain insights on past changes in productivity in these two different depositional environments. Higher sedimentation rates found at the head of the fjord result from the combination of a shallower water column and a restricted circulation by the occurrence of a sill. Additionally, sediment mixing depths estimated from $^{210}$Pb data suggest that suboxic conditions may dominate the bottom water and the sediment-water interface in this location.

Productivity of the Puyuhuapi fjord during the last century was characterized by a constant increase from the late 19$^{th}$ century to the early 1980s, then decreased until the late-1990s, and then rose again to present-day values. The influence of rainfall on productivity was most noticeable during periods of low rainfall, which coincided with decreased overall productivity within the Puyuhuapi fjord. Simultaneous variations in productivity and rainfall in the study area suggest that marine productivity could respond to atmospheric-oceanic interactions at a local scale. At a regional scale, marine productivity of the area may be related to other large-scale processes such as the El Niño Southern Oscillation.

## 1. Introduction

Pelagic productivity plays an important role in the transfer of carbon from the atmosphere to the sediments through the biological pump (Berger et al., 1989). Although organic matter preserved in marine sediments is mainly derived from exported material biosynthesized by marine organisms inhabiting the ocean's surface waters, terrestrial organic matter can also be found along continental margins (e.g., Wakeham and Lee, 1993; Hedges and Keil, 1995; Hedges et al., 1997). The flux of organic matter to marine sediments is controlled by primary production, heterotrophic degradation, water column depth, and advective transport (e.g. Wakeham and Lee, 1993), whereas preservation in the sedimentary record is mainly affected by sediment and organic matter accumulation rates, bottom water oxygen, organic matter sources, and adsorption onto mineral grains (e.g. Hedges and Keil, 1995). The biological signature preserved in the sedimentary record, discrete organisms as well as elemental and molecular proxies, is useful to determine past changes in productivity and to infer possible causes of its variation.

The sediment geochemistry of the Chilean fjords (south of 41°S) has received attention in the last decade, mainly with the support of the Chilean Cimar-Fiordos Program (National Oceanographic Committee) in the area between Puerto Montt (42ºS) and Cape Horn (56ºS). These studies, however, have focused mostly on the geochemistry of surface sediments (e.g., Ahumada et al., 1996; Silva et al., 1998; Silva and Prego, 2002). Downcore records of organic compounds are scarce (e.g., Rojas and Silva, 2003) and a lack of studies on paleoceanographic processes is evident.

Relatively high sedimentation rates characterize the Chilean fjord region (Rojas, 2002; Salamanca and Jara, 2003) and allow recovery of records with decadal or sub-decadal resolution, favoring paleoceanographic studies, as a result of ocean-atmosphere interactions occurring at those time scales.

This area is under the influence of the main Southern Hemisphere atmospheric circulation pattern, the Southern Westerlies, which in turn, are closely linked to changes within the tropical climate system and climate conditions in coastal Antarctica (e.g. Lamy et al., 2001). Thus, this region is critical for clarifying the synchronicity in the interhemispheric timing of high latitude climate change and its connections with tropical and subtropical areas. Moreover, the combination of geographical location (see below) and high primary productivity (e.g., Astoreca et al., 2002) makes this area suitable to study changes in past export production originating from changes in both the paleo-Patagonian ice caps and the globally important Southern Ocean. The main anthropogenic influence in the area started with the establishment of the first towns in Chile's XI region (~ 46-46°S) in the early XX century; industrial activity began in the last decade with rapidly growing salmon farming.

This study addresses issues of paleoceanography and climate change during the last century in a still-pristine area influenced by the Westerlies and which will undergo significant anthropogenic alterations in the near future as salmon farming expands. We present the first reconstruction of changes in export production from the Puyuhuapi fjord and show that the most remarkable decreases in overall productivity seem to be associated with periods of negative rainfall anomalies in the region, and suggest a connection with climatic systems of lower latitudes.

### *1.1 Study Area*

The Puyuhuapi fjord is located in northern Patagonia (XI region), in Chile's southern fjord area (~44°50'S). Its basin has a NE-SW orientation (Fig. 1a) and water depths that vary from 50 meters at the head of the fjord to 300 meters in the center section (Araya, 1997). The Ventisquero Sound is part of the northernmost end of the Puyuhuapi fjord, where the Galvarino Pass divides and connects the

northern and southern sections of the sound (Fig. 1b). The Galvarino Pass represents a coastline constriction, decreasing the width of the sound from about 2000 m to nearly 200 m, and changing the depth from 40 m on the northern side to 8 m in the shallowest section of the sill, and to 80 m south of the pass (Valle-Levinson et al., 2001). Fresh water into the Puyuhuapi fjord is mainly supplied by the Cisnes River (~ 182 $m^3$ $s^{-1}$), located in the middle section of the fjord and next to Puerto Cisnes. Fresh water to the Ventisquero Sound is mainly provided by the Ventisquero (~ 34 $m^3$ $s^{-1}$) and Pascua (no data available) rivers, both of them discharging in the northern side of the sill. The climate of the area is generally characterized by high precipitation (~ 3000 mm $yr^{-1}$) (DGA, 2003). High primary production has been measured in the water column (average in spring ~ 0.3 g C $m^{-2}$ $d^{-1}$; Astoreca et al., 2002). Surface sediments have been characterized as fine (silty-clay) and organic-rich, with values up to 3.8% of organic carbon ($C_{org}$) and 0.4% of organic nitrogen in some areas (Silva et al., 1998). Water column anoxia has not been reported for the fjord area, although measurements of dissolved oxygen in the water column have never included waters near the sediment-water interface (within ~ 1 m). Nonetheless, oxygen concentrations as low as 1.5 ml $L^{-1}$ have been detected at about 10 m above the sediments at the head of the Puyuhuapi fjord (Silva et al., 1997).

## 2. Materials and Methods

### *2.1 Sampling*

Sediment samples were obtained from the Puyuhuapi fjord (~ 44°49’S, 72° 56’W) (Figs. 1a, b). Two box-cores were recovered during the Cimar-7 Fiordo expedition (November 2001) aboard AGOR Vidal Gormaz: Station 40, located at the center of the fjord (44°49.39'S; 72°56.02'W; 270 m depth), and Station 35, located at the head of the fjord (Ventisquero Sound) (44°21.37'S; 72°34.82'W; 56 m

depth). Each box-corer was sub-sampled onboard using PVC tubes of 7 cm diameter to obtain sub-cores of about 30 cm length. These sub-cores were extruded and sectioned into 1 cm intervals, stored in plastic bags, and frozen at –20ºC until analyses in the laboratory.

>>>>>> *Figure 1 here*

*2.2 Sedimentation, mass accumulation rates, and geochronology*

Sedimentation rates, mass accumulation rates, and sediment age were determined from the excess (unsupported) $^{210}$Pb distribution. The analysis of $^{210}$Pb was carried out by alpha spectrometry of its daughter $^{210}$Po according to Flynn (1968). Unsupported $^{210}$Pb activities were determined from the total $^{210}$Pb minus the asymptotic activity at depth, assumed to be in equilibrium with $^{226}$Ra in the sediment (Appleby and Oldfield, 1978; Cochran et al., 1998; Lewis et al., 2002). Sedimentation and mass accumulation rates were calculated according to Christensen (1982) based on the general advection–diffusion equation assuming an exponential sedimentation rate and bulk sediment density in the absence of mixing (Eq. 1):

$$\rho = \rho_\infty - \rho_1 \times e^{-az} \qquad \text{(Eq. 1)}$$

where $\rho$ is the bulk density (g cm$^{-3}$); $\rho_\infty$ is the bulk sediment density at infinite depth; $\rho_1$ is the difference in bulk density between the surface and $\rho_\infty$; $a$ is the compaction coefficient (cm$^{-1}$); and z is the sediment depth. Equation 2 was used to estimate the mass accumulation rate $r$ under steady state conditions:

$$A = A_0 \exp(-\lambda/r\ [\rho_0 z - (\rho_1/a)(1-e^{-az})]) \qquad \text{(Eq. 2)}$$

where $\lambda$ is the decay constant of $^{210}$Pb (0.031 yr$^{-1}$) and A and $A_0$ are the unsupported downcore and initial $^{210}Pb_{xs}$ activities, respectively (dpm g$^{-1}$). We established the chronology for the sediment cores

using the constant rate of supply (CRS) method (Appleby and Oldfield, 1978; Turekian et al., 1980; Cochran et al., 1998) which assumes a constant flux of unsupported $^{210}$Pb. This allowed us to estimate sediment ages downcore while considering changes in sedimentation rates. The age at any depth in the core was calculated from equation 3:

$$t_z = \ln (Q_0/Q_z) / \lambda^{210} \quad \text{(Eq. 3)}$$

where $Q_0$ is the excess $^{210}$Pb inventory in the core (dpm cm$^{-2}$), calculated as $\Sigma A_i \rho_i h$, where h is the thickness of the interval (cm); $Q_z$ is the excess $^{210}$Pb inventory below depth z; and $A_i$ is the excess $^{210}$Pb activity.

Sedimentation rates and ages were estimated only below the mixing layer, where the effect of bioturbation is negligible. Standard deviations for the $^{210}$Pb inventories were determined by propagating the counting uncertainties as well as the error of the estimated background (Bevington and Robinson, 1992).

### *2.3. Grain size*

Wet sediments were resuspended in 35% NaCl and divided into two fractions using a 63µm sieve. Water was separated from each fraction by centrifugation (2 min. at 2500 rpm). Samples were then dried at 60°C in an oven until reaching a constant weight. Additionally, the < 63µm fraction was analyzed using an Elzone 282PC micro particle counter. Wet samples were resuspended in 35% NaCl and sonicated 5 minutes before analysis.

### *2.4. Organic carbon*

Organic carbon ($C_{org}$) analysis was performed by high temperature oxidation with a TEKMAR DOHRMANN elemental analyzer. Samples were ground and freeze-dried, and then

acidified with 15% HCl (until effervescence subsided) in glass vials to remove inorganic carbon. The remaining acid was evaporated at 80°C for 2 hours. Acetanilide (Mallinckodt Baker) was used as a reference standard.

*2.5. Chlorins*

Subsamples of ~ 0.2 g of wet sediment were mixed with 5 mL of 90% acetone in 15 mL polypropylene centrifuge tubes, homogenized using a Vortex mixer and sonicated for 10 min. The liquid phase (supernant) was recovered after centrifugation at 3000 rpm for 5 min and transferred to 20 mL vials (3x). Samples were measured using a Turner Design 10.005 fluorometer after dilution, before and after acidification with 10% HCl. Chlorin concentration was calculated as the sum of chlorophyll-*a* and phaeopigment concentrations.

*2.6. Proteins*

Proteins were measured as total hydrolyzable amino acids (THAA). A sediment subsample of 0.1 g was placed in 1.5 mL of $N_2$-purged hydrolysis solution (7N HCl, 0.1% phenol, 10% TFA) for 1.5 h at 150$^{o}$C. The solution was then neutralized with NaOH. Aliquots of the neutralized solution were derivatized with *o*-phthaldialdehyde and 2-mercaptoethanol according to Mopper and Lindroth (1982) with some modifications (Pantoja and Lee, 1999). Precolumn derivatization was carried out with a Shimadzu SIL-10A autoinjector and samples were analyzed on a Shimadzu HPLC using an on-line fluorescence detector (Shimadzu RF-10$A_{XL}$) set at 330 nm (excitation) and 450 nm (emission). Separation of 15 protein amino acids was performed on an Alltech $C_{18}$ column using a gradient program of 0.05 M sodium acetate and 5% tetrahydrofurane pH 5.7, and methanol.

*2.7. Biogenic silica (Si-opal)*

Biogenic silica was analyzed according to Mortlock and Froelich (1989). A freeze-dried sediment subsample of 25 mg was mixed with 10 mL $H_2O_2$ and 5 mL 1N HCl in centrifuge tubes. Samples were sonicated for 30 min and 10 mL of Milli-Q water were added. Each tube was centrifuged at 4300 rpm for 5 min, the supernatant was removed, and the sediment dried overnight at 60°C. A 40 mL aliquot of 1M NaOH was added to each tube and sonicated at 85°C for 6 h. Samples were centrifuged again at 4200 rpm for 5 min before measuring at 812 nm. Biogenic opal data are reported as Si-opal.

*2.8. Diatoms*

About 1 g of dry sediment was oxidized with 25% $H_2O_2$ and HCl. A 0.2 mL subsample was deposited and decanted on a glass slide and fixed with Hyrax resin (Rebolledo et al., accepted). About 300 diatom valves per slide were identified and counted using a Zeiss Axioskop 2 plus microscope with phase contrast illumination at 1000X magnification. Diatom identification and taxonomy were based on Cupp (1943), Rivera (1981), Round et al. (1990), and Thomas (1997).

*2.9. Diagenetic models*

In order to use $C_{org}$, chlorins, and THAA profiles, together with diatom and opal data as productivity indicators, we corrected the observed concentrations to account for post-deposition diagenesis according to Zimmerman and Canuel (2002). Only vertical profiles from Station 35 were corrected for the diagenetic effect since they showed exponential-type decay with depth, which suggests steady state diagenesis.

Reactivity of sedimentary $C_{org}$, chlorins, and THAA is represented by their apparent degradation first-order rate constant (*k*'). The rate constant k' was obtained as the slope of the relationship between

-ln [($C_t$ - $C_\infty$) / $C_o$] and time, where $C_t$ is the concentration of the organic component at time *t*; $C_\infty$ represents the asymptotic concentration in the vertical profile; and $C_o$ represents the concentration of the metabolizable component at the sediment surface.

Thus, assuming steady-state first-order degradation kinetics (Berner, 1980), the modeled profile for a metabolizable organic component of concentration $C_m$ deposited at time *t* can be calculated as:

$$C_{m_t} = C_o e^{-k't} + C_\infty \quad \text{(Eq. 4).}$$

Thus, the degradation or component loss ($C_{lost\text{-}t}$) for any sample deposited *t* years ago was estimated as:

$$C_{lost\text{-}t} = C_o - C_{m_t} \quad \text{(Eq. 5)}$$

and the degradation-corrected concentration ($C_{corr\text{-}t}$) for a sample of concentration $C_t$, is found by:

$$C_{corr\text{-}t} = C_t + C_{lost\text{-}t} \quad \text{(Eq. 6),}$$

all according to Zimmerman and Canuel, 2002.

*2.10. Calculation of accumulation rates*

Accumulation rates of proxies were calculated as $\rho$ x $C_t$ x *z/t* (McCaffrey and Thompson, 1980). Accumulation rates of $C_{org}$, chlorins, and THAA at Station 35 were calculated from degradation-corrected concentrations ($C_{corr\text{-}t}$).

*2.11. Productivity index*

A productivity index was calculated based on the normalized (see below) accumulation rates of degradation-corrected concentration of $C_{org}$, chlorins, THAA, and Si-opal, and marine diatoms, as proposed by Hebbeln et al. (2002). Accumulation rates of each property profile were normalized to a 0-1 scale by subtracting the minimum value from the individual down core measurements, and then dividing the resulting value by the maximum minus the minimum value (Hebbeln et al., 2002). The

productivity index corresponds to the average of all the normalized accumulation rates of proxies (on a 0-1 scale).

We tested the reliability of our results and its application as a paleoproxy by correcting for the diagenetic effect using minimum and maximum k' values from literature, and comparing them with our results. Reported k' values for comparable environments (fjords, estuaries and bays) for $C_{org}$ are 0.003-0.053 $y^{-1}$ (Haugen and Lichtentaler, 1991), 0.01 $y^{-1}$ (Farias et al., 1996), 0.013-0.05 $y^{-1}$ (Louchouarn et al., 1997), and 0.071-0.073 $y^{-1}$ (Rojas, 2002); k' values for THAA have been reported between 0.003-0.053 $y^{-1}$ in the Oslo fjord, Norway (Haugen and Lichtentaler, 1991). Even though the magnitude of corrected profiles changes as we use different k' values, the trend remains unaltered, nor did the shape or the general trend of the productivity index change (see below). Based on that, we used here the rate constants k' derived from our profiles instead of values from literature since our results for $C_{org}$ (0.036 $y^{-1}$) and THAA (0.028 $y^{-1}$) were within the range of those previously reported for environments of similar characteristics. We compared k' values for chlorophyll instead of chlorins because of the lack of reported data, and the trend was similar as above.

*2.12. Rainfall*

Historical rainfall data (1930 – present) between the areas of Puerto Aysén and Puerto Cisnes (Fig. 1) were obtained from the Chilean water resources office (DGA, 2003). Regional annual precipitation was calculated as the annual average of both cities, and rainfall anomalies from the averaged annual as precipitation minus the historical average, divided by the historical standard deviation. Smoothed anomalies were obtained as three running means.

## 3. Results

Sediment color at station 35 varied between grayish dark and grayish olive and presented a clay-silt texture with an organic-rich layer with plant debris below 30 cm. Strong $H_2S$ smell was noticed during subsampling. Sediment at station 40 presented a moderate olive brown color and a clay-silt texture along the core, with a 4 cm thick sandy layer between 12 and 15 cm, and an organic-rich layer corresponding to terrestrial plant debris below 22 cm.

### *3.1 Sedimentation rates and chronology*

Unsupported (excess) $^{210}Pb$ activities ($^{210}Pb_{xs}$) were estimated by subtracting the activity in equilibrium with $^{226}Ra$ (supported), which is usually constant with depth (Fig. 2a, b). The supported activity was estimated as the average activity in the last two depth-intervals for Station 35 (1.42 ± 0.04 dpm $g^{-1}$), due to the fact that core 35 did not show a good exponential fit (Table 1), and from the exponential fit of the model for Station 40 (1.62 ± 0.28 dpm $g^{-1}$).

>>>>>> *Table 1 here*

>>>>>> *Figure 2 here*

The supported $^{210}Pb$ at Station 35 was reached at ~29 cm (Fig. 2a). However, the interval below 26 cm appears too old to be reasonable (Table 2). Thus, the $^{210}Pb$ chronology presented here for Station 35 refers to the upper 26 cm and suggests that the core encompasses the period from 1899 AD to the present (Table 2). The sand layer between 12 and 15 cm at Station 40 interrupted the activity

distribution due to the introduction of material with lower $^{210}$Pb activity (Fig. 2b). $^{210}$Pb activity below the sand layer was fairly constant and thus considered as supported activity. $^{210}$Pb activities reached constant levels at 10 cm; however, dating of the last three sections before the sand layer may be regarded as spurious due to a poorly defined background. Therefore, we considered dating from 1948 AD (i.e., the lower limit of interval 6-7 cm) as appropriate (Table 2).

>>>>>> *Table 2 here*

Homogeneous surface activities were found in the upper 5 cm at Station 35, whereas an irregular distribution in the top three centimeters was detected at Station 40. Based on $^{210}$Pb methodologies, sedimentation rates at the sediment surface were estimated as 0.74 ± 0.08 cm $y^{-1}$ for Station 35 and 0.25 ± 0.07 cm $y^{-1}$ for Station 40 (Table 1), assuming a constant mass accumulation rate in both cases.

*3.2. Grain size*

Grain size analysis was performed for both cores, although the > 63μm fraction was not analyzed for Station 35 due to limitations in the amount of available sediment material. The silt-clay fraction at station 35 ranged between 5.5 to 8 μm, and a general trend of increasing grain size was observed down to ~ 15 cm (Fig. 2c). Size range of the silt-clay fraction at Station 40 was narrower than at Station 35 and varied between 5 and 7 μm with a minimum at 14 cm associated with the sand layer, which can be considered as the core of the turbidite (Fig. 2d). Grain size values at station 40 showed a higher contribution of the silt-clay fraction (< 63 μm), which accounted for ~ 70%, except between 11 and 15 cm where the sand layer (> 63 μm fraction) consisted of 84% (Fig. 2d).

*3.3. Surface sediments and downcore distribution of proxies*

Organic carbon concentrations in surface sediments were similar at both stations (~ 18 mg $gdw^{-1}$) but the downcore pattern differed (Figs. 3a, g). Average concentration throughout the core at station 35 decreased exponentially from 18 mg $gdw^{-1}$ at the sediment surface to a nearly constant value of ~11 mg $gdw^{-1}$ below 16 cm (Fig. 3a). These values were almost half the concentration values observed at the bottom of the core of Station 40 (Figs. 3a, g). $C_{org}$ at station 40 varied between 14 and 33 mg $gdw^{-1}$, reaching a maximum at 3 cm depth with the lowest value within the sand layer (Fig. 3g).

Sediment chlorine concentrations were higher at the surface (3x) and downcore (1.5x) at Station 35 than at Station 40 (Figs. 3b, h). The downcore pattern exhibited a marked exponential decay with depth from 130 µg $gdw^{-1}$ at the sediment surface to 26 µg $gdw^{-1}$ at 8 cm in Station 35 (Fig. 3b). Chlorine values remained fairly constant downcore. Chlorins at Station 40 exhibited the highest concentration at 4 cm (74 µg $gdw^{-1}$) and lowest values within the sand layer (<10 µg $gdw^{-1}$). Above and below the sand layer, values varied around 14 µg $gdw^{-1}$ (Fig. 3h).

THAA concentrations at Station 35 decreased with depth from 6.4 mg $gdw^{-1}$ at the surface to about 2.8 mg $gdw^{-1}$ below 16 cm (Fig. 3c). THAA concentrations were not measured at Station 40.

Biogenic opal concentrations in surface sediments were somewhat lower at Station 35 (40 mg $gdw^{-1}$) than at Station 40 (51 mg $gdw^{-1}$) (Figs. 3d, i). Downcore values at Station 35 ranged between 30 and 40 mg $gdw^{-1}$ in the upper 7 cm of the core, and between 30 and 58 mg $gdw^{-1}$ in the 8-32 cm interval (Fig. 3d). At Station 40, on the other hand, Si-opal ranged between 50 and 55 mg $gdw^{-1}$ from the sediment surface to 7 cm, and between 15 and 55 mg $gdw^{-1}$ from 8 to 23 cm, reaching the lowest value within the sand layer (Fig. 3i).

>>>>>> *Figure 3 here*

Abundance of marine diatoms in surface sediments at Station 35 ($1.9x10^7$ valves $gdw^{-1}$) was almost twice as high as at Station 40 ($1x10^7$ valves $gdw^{-1}$) (Figs. 3e, j), whereas the abundance of fresh water diatoms was almost an order of magnitude higher at Station 35 ($2x10^6$ valves $gdw^{-1}$) than at Station 40 ($0.6x10^6$ valves $gdw^{-1}$) (Figs. 3e, j) (see also Rebolledo et al., accepted). Downcore abundances at Station 35 showed a constant decrease in both profiles, although marine diatoms were, on average, 3.5 times more abundant than fresh water diatoms (Figs. 3e). At Station 40, both types of diatoms differed in their downcore concentration patterns, and a wide range in concentration values was observed (Fig. 3j). Marine diatoms varied between $2.3x10^6$ and $2.5x10^7$ valves $gdw^{-1}$ and presented the lowest values in the sand layer, while fresh water diatoms varied between $4x10^3$ and $2.7x10^5$ valves $gdw^{-1}$ with the lowest values in the top two centimeters (Fig. 3j). At Station 35, marine diatoms represented ~ 85% of the total diatom assemblage in the top two centimeters; they remained rather constant down to 18 cm (76%), and decreased to a minimum value of 58% in the 24-25 cm interval (Fig. 3f). At Station 40, marine diatoms represented between 73 and 95% of total diatoms with the highest values in the top two centimeters (Fig. 3k). The average contribution of fresh water diatoms at Station 35 (21%) was higher than at Station 40 (14%), and the lowest values at both stations were found in the top two centimeters.

### *3.4. Diagenetic correction of $C_{org}$, chlorins, and THAA (Station 35)*

Organic carbon, chlorins, and THAA profiles from Station 35 were corrected for diagenetic effects according to Zimmerman and Canuel (2002) and are plotted against estimated age in Fig. 4. $C_{org\text{-}corr}$ remained fairly constant, close to 18 mg $gdw^{-1}$ between AD 1890 and 1990, and then dropped to its lowest values (15 mg $gdw^{-1}$) in the 1990s (Fig. 4a), whereas $Chlorins_{corr}$ fluctuated between 120 and 130 μg $gdw^{-1}$ (Fig. 4b). The corrected profile of THAA varied between 4 and 8 mg $gdw^{-1}$ with the

highest concentrations (~ 7 mg $gdw^{-1}$) occurring before 1990 (Fig. 4c). For Station 40, we did not correct organic carbon and chlorins for the diagenetic effect (THAA were not measured) because dating at this station was limited by the presence of a sand layer which affected the dating of background values of organic proxies, and because vertical profiles of carbon and chlorins did not follow an exponential-type decay with depth, suggesting non-steady state diagenesis. In fact, both profiles at Station 40 presented a subsurface peak at the 3-4cm depth interval (Figure 3g, h).

>>>>>> *Figure 4 here*

*3.5. Accumulation rates*

Dating of sediments was most reliable down to 26 cm at Station 35. Calculations of accumulation rates presented here encompass the 1890-2001 period (Fig. 5). Because of the presence of the sand layer and the fact that we did not correct $C_{org}$ and chlorins for the downcore diagenetic effect (see above), accumulation rates of proxies at Station 40 were only estimated for the sediment surface (see open diamonds in Figure 5). In general, surface accumulation rates at Station 35 were 1.5, 6, 1.5, 3 and 7 times higher than at Station 40 for $C_{org}$, chlorins, Si-opal, and marine and fresh water diatoms, respectively (Fig 5).

All accumulation rates showed a linear increase from AD 1890 to the early 1980s (Fig. 5). From the 1980s until the present, $C_{org}$ and chlorins remained relatively constant (Figs. 5a, b), whereas THAA and Si-opal decreased (Figs. 5c, d). Marine and fresh water diatoms remained rather constant although somewhat erratic in the youngest section of the record (Fig. 5e, f).

>>>>>> *Figure 5 here*

*3.6. Paleoproductivity index*

The productivity index calculated for Station 35, based on diagenesis-corrected profiles of $C_{org}$, chlorins and THAA, Si-opal, and marine diatoms showed that the export production in the Seno Ventisquero was marked by a constant increase from AD 1890 to the early 1980s. Decreased productivity was observed from 1980 to the late nineties, after which an increase was detected toward the present (Fig. 6a).

>>>>>> *Figure 6 here*

*3.7. Rainfall*

Rainfall anomalies (with respect to the historical average of the time series) were characterized by marked periods of lower values between AD 1934-1956, 1972-1980, and 1994-2001, and periods of higher rainfall were observed between AD 1957-1971 and 1981-1994 (Fig. 6b).

## 4. Discussion and Conclusion

*4.1. $^{210}$Pb distribution, sedimentation rates, and geochronology*

In general, $^{210}$Pb surface activities and depth distribution in the Puyuhuapi fjord are similar to those reported for other Chilean fjords (Salamanca and Jara, 2003). Sedimentation rates determined in this study (0.25-0.74 cm yr$^{-1}$ at the sediment surface) were in the range of those reported previously for the area by Rojas (2002) (0.26-0.33 cm yr$^{-1}$) and Salamanca and Jara (2003) (0.14-0.47 cm yr$^{-1}$) (Table 1). The presence of a sand layer between 11 and 15 cm at Station 40 with lower $^{210}$Pb activities could be the result of a rapid deposition event (turbidite) with removal of sediment.

The differences in surface sedimentation and mass accumulation rates observed between stations 35 (0.74 cm $yr^{-1}$ and 0.22 g $cm^{-2}$ $yr^{-1}$) and 40 (0.25 cm $yr^{-1}$ and 0.11 g $cm^{-2}$ $yr^{-1}$) may be the result of differences in topography and circulation within the depositional environments. Station 40 is located in the center of the Puyuhuapi fjord, in a relatively hydrographically unstable environment (Fig. 1a). Station 35, on the other hand, is located in the shallow and restricted Ventisquero Sound (head of the fjord) separated from the fjord by a sill, and influenced by the Ventisquero and Pascua rivers (Fig. 1; see Study Area above). Thus, the environment at Station 35 seems to be more stable and sedimentation rates may be enhanced due to the proximity to river deposition. Differences in grain size can be ruled out, as both stations are dominated by the silt-clay fraction (Silva et al., 1998), except for the sand layer at Station 40. Furthermore, the mean size of the < 63 μm fraction was similar at both stations (Figs. 2c, d).

Homogeneous profiles of $^{210}Pb$ activity for the top 5 and 3 cm of Stations 35 and 40, respectively, could be the result of biological mixing by bioturbation (Figs. 2a, b). These mixing depths are similar to those reported for other coastal areas where bioturbation is diminished by low-oxygen water, and they are lower than in better oxygenated areas (Table 5 in Smith et al., 2000). Although other factors such as organic matter quality can also affect bioturbation (e.g., Smith et al., 2000), we suggest that suboxic conditions may dominate bottom waters and the sediment-water interface in the area surrounding Stations 35 and 40 in the Puyuhuapi fjord. CTDO measurements 10 m above the bottom show that the lowest oxygen concentration (1.5 ml $L^{-1}$) has been detected at the head of the Puyuhuapi fjord (Silva et al., 1997). In addition, high concentrations of Fe (II) in surface sediments of the Aysén fjord and the channels Costa and Elefantes (Fig. 1) may result from iron reduction during anaerobic degradation of organic matter (Pinto and Rivera, submitted).

*4.2. Paleoproductivity*

Accumulation rates at the sediment surface for all proxies were greater at Station 35 than at Station 40 (Fig. 5). Available information indicates that, although primary production may vary between fjords, differences within the Puyuhuapi fjord during spring are less than 25% (Astoreca et al., 2002). Therefore, we suggest that differences in accumulation rates between both stations may be attributed to: 1) Differences in water column depth (270 m for Station 40 vs. 56 m for Station 35) and associated heterotrophic degradation of organic material in the water column; i.e., sinking particles at Station 40 will undergo longer exposure to degradation and remineralization in the water column and/or 2) geomorphology of the northern side of Ventisquero Sound, where Station 35 is located; the site is located in an enclosed and stable area where sedimentation is enhanced. Cáceres and Valle-Levinson (2004) reported an anticlockwise rotation of the mean flow in the northern side (Station 35) of the Galvarino pass in the Ventisquero Sound, probably influenced by river discharges. They also proposed that recirculation in the northern section of the Ventisquero Sound might constitute a water retention area, where the dispersion of particulate material is restricted by the presence of the sill in the Galvarino pass and by the longer residence time of the water. Even though we can not rule out better preservation of organic material at Station 35, given its apparent greater degree of hypoxia, we do not have conclusive evidence for this. However we can rule out a higher input of refractory terrestrial organic matter at Station 35 by higher freshwater influence due to its proximity to the Ventisquero river mouth. Sepúlveda et al. (in prep.) found that Stations 35 and 40 are comparable in terms of terrestrial organic carbon content.

Total diatom abundance in surface sediments of the Puyuhuapi fjord was an order of magnitude lower than in similar environments such as the Effingham Inlet in Canada (Murray et al., 2003).

Downcore diatom concentrations fall within the range of those recorded in Saanich Inlet, Canada (McQuoid and Hobson, 1997, 2001; Johnson and Grimm, 2001). The Si-opal content was lower than that found in Saanich Inlet, where values up to 45% have been reported (Johnson and Grimm, 2001; McQuoid and Hobson, 1997, 2001). Since $C_{org}$ contents of our study were comparable to those reported for Saanich Inlet and C/N ratios were much higher, dilution by terrestrial organic matter may play an important role in the Chilean fjords. Sepúlveda et al. (in prep.) found that up to 50% of organic matter in surface sediments of Stations 35 and 40 in the Puyuhuapi fjord would be originated by terrestrial sources.

Accumulation rates of proxies define two distinct periods: AD 1890-1980 and 1980-2001 (Fig. 5). Correlations among proxies were estimated separately for these two periods (Table 3). Between 1890 and 1980, all proxies were highly correlated ($r > 0.8$, $p < 0.05$), although none were significantly correlated with rainfall anomalies (Table 3). Between AD 1980 and 2001, chlorins were significantly correlated with THAA and fresh water diatoms, and fresh water diatoms with rainfall (Table 3). All proxies reveal an increase in accumulation rates from the late 19$^{th}$ century to the early 1980s at Station 35 (Fig. 5). From 1980 to the present, the pattern differs among proxies. For example, while diatom accumulation rates remained high and fairly constant up to the mid-1990s, THAA accumulation rates decreased, and Si-opal decreased abruptly during the early 1980s. $C_{org}$ values and chlorins, on the other hand, did not show any significant changes (Fig. 5). Considering that the top 5 cm of the sediment column (~10 years) are diagenetically active, and that bioturbation by benthic organisms may have modified and mixed the sedimentary signal, paleo-interpretation of the period 1980-2001 must be taken with caution. For instance, although we noted that both THAA and Si-opal remained constant from the early 80s until the present, we focused only on the general trend (see above).

We propose that the decrease of Si-opal could be the result of a change in the diatom community promoted by environmental forcing. Because different species of diatoms respond differently to changes in physical, chemical, and biological environmental conditions, such as light intensity, nutrient availability, turbulence, and grazing (e.g., Lalli and Parsons, 1997; Smetacek, 1999), a change in species composition of the diatom assemblage may occur (e.g., from robust to fragile diatoms).

Highly significant correlations ($r \geq 0.8$, $p < 0.05$) between corrected organic proxies and marine and fresh water diatoms were observed from AD 1890 to 1980 (Table 3), suggesting that $C_{org}$, chlorins, THAA, and Si-opal represent phytoplanktonic productivity in the sedimentary record. These results agree with other findings for the Chilean coast between 22-45°S, where a good agreement between opal content and diatom concentration in core-top sediments was found (Romero and Hebbeln, 2003), and accumulation rates of organic carbon correlate with present-day productivity (Hebbeln et al., 2000). However, low correlations between proxies were observed from 1980 to the present (Table 3), suggesting that sources of organic matter other than phytoplanktonic production, such as highly refractory carbon from weathering of deforested land and organic waste from aquaculture activity after 1990 could be influencing the record.

The non-significant correlation between marine and fresh water diatoms from 1980 to the present (Table 3) implies that both groups may not respond to environmental forcing in a similar way. Only fresh water diatoms were well-correlated with rainfall anomalies ($r = 0.76$, $p < 0.05$). Therefore, other factors such as glacial melting could be influencing nutrient discharge by rivers, which can be noted during cold periods, as was seen during the last two advances of the Frías glacier (41°S) in 1940 and 1977 (Villalba, 1994 and references therein), when freshwater diatom accumulation rates were rather low.

>>>>>> *Table 3 here*

According to the paleoproductivity index, export production in the Ventisquero Sound increased constantly from AD 1890 to the early 1980s, and then decreased until the late nineties when a recovery to conditions similar to those found in the mid-eighties returned (Fig. 6a). The most remarkable decreases in productivity were associated with periods of negative rainfall anomalies (Figs. 6a, b), with a subsequent decrease of runoff reflected in the diminished accumulation rates of fresh water diatoms (Fig. 5f). This indicates that the largest influence of rainfall on productivity is mainly noticeable during periods of decreased overall runoff, compared to those periods with normal and positive anomalies due to the high year-round precipitation in the area (~ 3000 mm $yr^{-1}$; DGA, 2003). In general, positive anomalies of rainfall are coincident with stable or high productivity, whereas negative rainfall anomalies correlate with decreased productivity.

Hebbeln et al. (2000) suggested that the high productivity found south of 40°S could be supported by the iron-limited high nutrient/low chlorophyll waters of the Antarctic Circumpolar Current (ACC) and riverine micronutrients. Strong riverine input is expected due to high precipitation in this area. Precipitation in Southern Chile is mostly controlled by the Westerlies (Aceituno, 1988), which may be affected by latitudinal and/or strength variations in the South Pacific Anticyclone, as observed during El Niño events (Ruttland and Fuenzalida, 1991). It has been proposed that past changes in productivity in central and southern Chile are promoted by latitudinal shifts in the position of the Westerlies and migration of the ACC, due to changes in precipitation and macronutrient supply (Marchant et al, 1999; Hebbeln et al., 2002). Other teleconnections have been described as well. For instance, Villalba (1994) found that humid winters in central Chile are followed by warm summers in Patagonia and vice versa, similar to El Niño and La Niña events (Aceituno, 1988; Rutlland and Fuenzalida, 1991). Thus,

appropriate records from Patagonia may track ENSO at decadal scales showing combined warm and cold events within decades (Villalba, 1994). A preliminary comparison of our records from the late 1930s, with climatic events occurring in lower latitudes of Chile and South America, showed correspondence of high and low productivity with positive and negative ENSO phases, for the last 60 years (MEI and ENSO-3 indexes, data not shown). We propose that during weak El Niño or La Niña events, and during extended periods without a clear dominance of either event, productivity could be controlled by local mechanisms. Further studies of paleoproductivity and paleoclimate encompassing other areas within the fjord system are necessary to identify the relationships between marine primary production at this latitude and climatic forcing from lower latitudes.

## 5. Acknowledgements

We are grateful to the Ministerio de Hacienda de Chile (Chilean Ministry of Treasury) and the National Oceanographic Committee (CONA) for financial support to carry out the Cimar-7 Fiordo Program (Grant C7F 01-10 to Silvio Pantoja). We also thank the Navy's Hydrographic and Oceanographic Service (SHOA) and the captain and crew of the AGOR Vidal Gormaz for their professional help during field work; the EULA Center (University of Concepción) for making available a box-corer, fluorometer, and micro particle counter; and the FONDAP-COPAS Center, and Grant 200.031.085-1 (UdeC) for financial support. We extend our acknowledgements to P. Vera for logistical assistance before and during the cruise, L. Nuñez for laboratory support, T. Aguayo for TOC measurements, A. Araneda for grain size analysis, and M. Cáceres for the Ventisquero Sound map used in Fig. 1b. J. Sepúlveda was funded by a scholarship from the Graduate School of the University of Concepción and by the FONDAP-COPAS Center. Additional support was given by Fundación Andes through the Woods Hole Oceanographic Institution/University of Concepción agreement. The manuscript benefited from the comments of two anonymous reviewers.

## 6. References

Aceituno, P., 1988. On the functioning of the Southern Oscillation in the South American sector. Part 1: Surface climate. Monthly Weather Review 116, 505-524.

Ahumada, R., Rudolph, A., Silva, N., 1996. Contenido de carbono total, carbono orgánico, carbono inorgánico, nitrógeno orgánico y fósforo total, en los sedimentos de los fiordos de Campos de Hielo Sur. Ciencia y Tecnología Marina 19, 123-132.

Appleby, P.G., Oldfield, F., 1978. The calculation of lead-210 dates assuming a constant rate of supply of unsupported $^{210}$Pb to the sediment. Catena 5, 1-8.

Araya, J.F., 1997. Perfiles geomorfológicos de los fiordos y depresión longitudinal de norpatagonia. Ciencia y Tecnología del Mar 20, 3-20.

Astoreca, R., Pizarro, G., Paredes, M.A., Uribe, P., Montecino, V., 2002. Relación entre patrones espaciales de productividad y la abundancia y estructura de tamaños del fitoplancton en sistemas de fiordos y canales de la XI Región. Comité Oceanográfico Nacional. Resultados preliminares del crucero CIMAR Fiordo 7, 77-88.

Berger, W.H., Smetacek, V.S., Wefer, G., 1989. Ocean productivity and paleoproductivity-an overview. In: Berger, W.H., Smetacek, V.S., Wefer, G. (Eds.), Productivity of the Ocean: Present and Past. Dahlem Workshop Reports, Wiley Interscience, Chichester, pp. 1-34.

Berner, R.A., 1980. A rate model for organic carbon decomposition during bacterial sulfate reduction in marine sediments. Biogeochemistry of organic matter at the sediment–water interface. CNRS International Colloquium, pp. 35–44.

Bevington, P., Robinson, K., 1992. Data reduction and error analysis for the physical science. USA: WCB/McGraw-Hill.

Cáceres, M., Valle-Levinson, A., 2004. Transverse variability of flow on both sides of a sill/contraction combination in a fjord-like inlet of southern Chile. Estuarine Coastal and Shelf Science 60, 325-338.

Christensen, E., 1982. A model for radionuclides in sediments influenced by mixing and compaction. Journal of Geophysical Research 87, 566-572.

Cochran, J.K., Frignani, M., Salamanca, M., Bellucci, L.G., Guerzoni, S., 1998. Lead-210 as a tracer of atmospheric input of heavy metals in the northern Venice Lagoon. Marine Chemistry 62, 15-29.

Cupp, E.E., 1943. Marine plankton diatoms of the west coast of North America. Bulletin , Scripps Institution of Oceanography 5, 1-238.

DGA, 2003. Dirección General de Aguas, Chile (www.dga.cl).

Farias et al., 1996. Reactivity and remineralization of total organic carbon and total nitrogen in anoxic sediments at Concepción Bay, Chile. Gayana Oceanologia 4, 117-127.

Flynn, W., 1968. The determination of low levels of Polonium-210 in environmental materials. Analytical Chemical Acta 43, 221-227.

Haugen, J., Lichtentaler, R., 1991. Amino acid diagenesis, organic carbon and nitrogen mineralization in surface from the inner Oslofjord, Norway. Geochimica et Cosmochimica Acta 55, 1649-1661.

Hebbeln, D., Marchant, M., Freudenthal, T., Wefer, G., 2000. Surface sediment distribution along the Chilean continental slope related to upwelling and productivity. Marine Geology 164, 119-137.

Hebbeln, D., Marchant, M., Wefer, G., 2002. Paleoproductivity in the southern Peru-Chile Current through the last 33000 yr. Marine Geology 186, 487-504.

Hedges, J.I., Keil, R.G., 1995. Sedimentary organic matter preservation: An assessment and speculative synthesis. Marine Chemistry 49, 81-115.

Hedges, J.I., Keil, R.G., Benner, R., 1997. What happens to terrestrial organic matter in the ocean?. Organic Geochemistry 27, 195-212.

Johnson, K.M., Grimm, K.A., 2001. Opal and organic carbon in laminated diatomaceous sediments: Saanich Inlet, Santa Barbara Basin and the Miocene Monterrey Formation. Marine Geology 174,159-175.

Lalli, C.M., Parsons, T.R., 1997. Biological oceanography an introduction, second edition. The Open University set Book, Butterworth-Heinemann, 314 pp.

Lamy, F., Hebbeln, D., Röhl, U., Wefer, G., 2001. Holocene rainfall variability in southern Chile: a marine record of latitudinal shifts of the Southern Westerlies. Earth and Planetary Science Letters 185, 369-382.

Lewis, R.C., Coale, K.H., Edwards, B.D., Marot, M., Douglas, J.N., Burton, E.J., 2002. Accumulation rate and mixing of shelf sediments in the Monterey Bay National Marine Sanctuary. Marine Geology 181, 157-169.

Louchouarn, P., Lucotte, M., Canuel, R., GagneÂ , J.-P., Richard, L.-P., 1997. Sources and early diagenesis of lignin and bulk organic matter in the sediments of the Lower St. Lawrence Estuary and the Saguenay Fjord. Marine Chemistry 58, 3-26.

Marchant, M., Hebbeln, D., Wefer, G., 1999. High resolution planktic foraminiferal record of the last 13,300 years from the upwelling area off Chile. Marine Geology 161, 115– 128.

McCaffrey, R., Thompson, J.A., 1980. Record of the accumulation of sediment and trace metals in the Connecticut salt marsh. Advances in Geophysics 22, 165-236.

McQuoid, M.R, Hobson, L.A., 1997. A 91-year record of seasonal and interannual variability of diatoms from laminated sediments in Saanich Inlet, British Columbia. Journal of Plankton Resesearch 19, 173-194.

McQuoid, M.R, Hobson, L.A., 2001. A Holocene record of diatoms and silicoflagellates microfossils of Saanich Inlet, ODP Leg 169 S. Marine Geology 174, 111-123.

Mopper, K., Lindroth, P., 1982. Diel and depth variations in dissolved free amino acids and ammonium in the Baltic Sea determined by shipboard HPLC analyses. Limnology and Oceanography 27, 336–347.

Mortlock, R.A., Froelich, P.N., 1989. A simple method for the rapid determination of biogenic opal in pelagic marine sediments. Deep-Sea Research 36, 1415-1426.

Murray, B.H, Pienitz, R., Thomson, R.E., 2003. Distribution of diatom surface sediments assemblages within Effingham Inlet, a temperate fjord on the West coast of Vancouver Island (Canada). Marine micropaleontology 48, 291-320.

Pantoja, S., Lee, C., 1999. Molecular weight distribution of protein in Long Island Sound sediments. Limnology and Oceanography 44, 1323-1330.

Pinto, L., Rivera, C. Distribución de Fe y Mn reducido en aguas intersticiales de fiordos y canales. Submitted to Ciencia y Tecnología del Mar.

Rebolledo, L., Lange, C., Figueroa, D., Pantoja, S., Muñoz, P., Castro, R. 20th century fluctuations in the abundance of siliceous microorganisms preserved in the sediments of the Puyuhuapi Channel (44°S), Chile. Accepted in Revista Chilena de Historia Natural.

Rivera, P., 1981. Beiträge zur Taxonomie und Verbreitung der Gattung *Thalassiosira* Cleve. Bibliotheca Pycologica 56, 1-220.

Rojas, N., 2002. Distribución de materia orgánica, carbono y nitrógeno, y diagénesis temprana en sedimentos de la zona de canales australes entre los golfos Corcovado y Elefantes, Chile. Tesis para optar al título de Oceanógrafo, Universidad Católica de Valparaíso, Valparaíso, Chile, 76 pp.

Rojas, N., Silva, N., 2003. Distribución espacial de textura, carbono y nitrógeno en sedimentos recientes en canales y fiordos Chilenos. Golfo Corcovado (43º 50' S) a Golfo Elefantes (46º 30' S), Chile. Ciencia y Tecnología Marina, 26, 15-31.

Romero, O., Hebbeln, D., 2003. Biogenic silica and diatom thanatocoenosis in surface sediments below the Peru-Chile Current: controlling mechanisms and relationship with productivity of surface waters. Marine Micropaleontology 48, 71-90.

Round, E.E., Crawford, R.M., Mann, D.G., (Eds.), 1990. The diatoms: biology and morphology of the genera. Cambridge University Press, Cambridge. 747 pp.

Ruttland, J., Fuenzalida, H., 1991. Synoptic aspects of the central Chile rainfall variability associated with the Southern Oscillation. International Journal of Climatology 11, 63-76.

Salamanca, M.A., Jara, B., 2003. Distribución y acumulación de plomo (Pb y $^{210}$Pb) en sedimentos de los fiordos de la XI región de Chile. Ciencia y Tecnología del Mar 26, 61-71.

Silva, N., Prego, R., 2002. Carbon and nitrogen spatial segregation and stoichiometry in the surface sediments of southern Chilean inlets (41°–56°S). Estuarine, Coastal and Shelf Science 55, 763-775.

Silva, N., Calvete, C., Sievers, H.A., 1997. Características Oceanográficas Físicas y Químicas de canales australes Chilenos entre Puerto Montt y Laguna San Rafael (crucero CIMAR-FIORDO 1). Ciencia y Tecnología del Mar 20, 23-106.

Silva, N., Maturana, J., Sepúlveda, J.I., Ahumada, R., 1998. Materia orgánica, C y N, su distribución y estequiometría, en sedimentos superficiales de la región norte de los fiordos y canales australes de Chile (crucero CIMAR-FIORDO 1). Ciencia y Tecnología del Mar 21, 49-74.

Smetacek, V., 1999. Diatoms and the ocean carbon cycle. Protist 150, 25-32.

Smith, C.R., Levin, L.A., Hoover, D.J., McMurtry, G., Gage, J.D., 2000. Variations in bioturbation across the oxygen minimum zone in the northwest Arabian Sea. Deep Sea Research 47, 227-257.

Thomas, A.C., (Ed.), 1997. Identifying Marine Phytoplankton. Academic Press. San Diego, 858 pp.

Turekian, K., Cochran, K., Benninger, L., Aller, R., 1980. The sources and sinks of nuclides in Long Island Sound. Advances in Geophysics 22, 129-163.

Valle-Levinson, A., Jara, F., Molinet, C., Soto, D., 2001. Observations of intratidal variability of flows over a sill/contraction combination in a Chilean fjord. Journal of Geophysical Research 106 (C4), 7051-7064.

Villalba, R., 1994. Fluctuaciones climáticas en latitudes medias de América de Sur durante los últimos 1000 años: sus relaciones con la Oscilación del sur. Revista Chilena de Historia Natural 67, 453-461.

Wakeham, S.G., Lee, C., 1993. Production, transport, and alteration of particulate organic matter in the marine water column. In: Engel, M.H., Macko, S.A. (Eds.), Organic Geochemistry. Plenum, New York, pp. 145-169.

Zimmerman, A.R., Canuel, E.A., 2002. Sediment geochemical records of eutrophication in the mesohaline Chesapeake Bay. Limnology and Oceanography 47, 1084-1093.

**Figure captions**

Figure 1. (a) Northern area of the XI region in southern Chile, showing the location of Station 40 in the Puyuhuapi fjord (black square and arrow) and other locations mentioned in the text; (b) Location of Station 35 (black square and arrow) in the Ventisquero Sound; (c) Longitudinal profile of the Puyuhuapi fjord, redrawn from Araya (1997). Map a) was obtained using www.aquarius.geomar.de/omc and map b) was modified from Cáceres and Valle-Levinson (2004).

Figure 2. Vertical distribution of $^{210}Pb_{xs}$ activity at Stations (a) 35 and (b) 40. Horizontal error bars are one standard deviation (1$\sigma$), obtained by propagating the counting uncertainties of $^{210}Pb$ and standard deviation of background. Vertical dotted lines are the supported activity. (c) Mean size distribution of grain size < 63 μm at Station 35. (d) Mean size distribution of grain size < 63 μm and percent fraction distribution of grain size above and below 63 μm at Station 40.

Figure 3. Downcore records at Stations 35 (upper panel) and 40 (lower panel); (a, g) total organic carbon (TOC) concentration (mg $gdw^{-1}$); (b, h) chlorin concentration (μg $gdw^{-1}$); (c) total hydrolyzable amino acid (THAA) concentration (mg $gdw^{-1}$); (d, i) Si-opal concentration (mg $gdw^{-1}$); (e, j) marine (filled circles) and fresh water (open circles) diatom concentrations (valves $gdw^{-1}$); and (f, k) percent contribution of marine and fresh water diatoms to total diatoms (%). Dashed vertical line in Figures a, b, and c represents the averaged value considered as background for diagenetic correction. Dashed area in upper panel represents a terrestrial plant debris rich layer. Dashed area in lower panel represents the interval of a sand layer. Gray area in upper panel represents the data excluded from dating, the

diagenetic correction and estimation of accumulation rates (see methods section). Gray area in lower panel represents the data excluded from dating.

Figure 4. Station 35. Downcore record of uncorrected (filled circles) and diagenesis-corrected (open circles) concentrations of TOC, chlorins, and THAA, and modeled profiles (solid line). (a) Total organic carbon (TOC) (mg $gdw^{-1}$); (b) chlorins (μg $gdw^{-1}$); (c) total hydrolyzable amino acids (THAA) (mg $gdw^{-1}$).

Figure 5. Station 35. Accumulation rates of (a) TOC (g $m^{-2}$ $yr^{-1}$); (b) chlorins (mg $m^{-2}$ $yr^{-1}$); (c) THAA; (d) Si-opal (g $m^{-2}$ $yr^{-1}$); (e) marine and (f) fresh water diatoms (valves $m^{-2}$ $yr^{-1}$). White diamonds represent surface accumulation rates at Station 40.

Figure 6. (a) Paleoproductivity index at Station 35 (as in Hebbeln et al., 2002), based on diagenesis-corrected profiles of $C_{org}$, chlorins and THAA, Si-opal, and marine diatoms. (b) Rainfall anomaly (bars) from Puerto Aysén and Puerto Cisnes since 1931; black line is a 3-year running mean (data from DGA, 2003).

Table 1. Model parameters used for estimating sedimentation rates according to Christensen (1982).

| Parameter | Core 35 | Core 40 |
|---|---|---|
| $\rho_\infty$ | 0.73 ± 0.05 | 0.69 ± 0.03 |
| $\rho_1$ | 0.39 ± 0.04 | 0.33 ± 0.06 |
| *a* | 0.09 ± 0.03 | 0.22 ± 0.08 |
| variance | 84% | 72% |
| $A_0$ | 3.45 ± 0.23 | 5.2 ± 0.40 |
| r | 0.22 ± 0.03 | 0.11 ± 0.03 |
| supported $^{210}$Pb | 1.42 ± 0.07 | 1.83 ± 0.13 |
| variance | 97% | 93% |
| Sedimentation rate (cm yr$^{-1}$) | 0.74 ± 0.08 | 0.25 ± 0.07 |

$\rho_\infty$ = bulk density at infinite depth (g cm$^{-3}$)

$\rho_1$ = difference in bulk density between the sediment surface and $\rho_\infty$ (g cm$^{-3}$)

a = compaction coefficient (cm$^{-1}$)

$A_0$ = $^{210}$Pb activity at the sediment-water interface (dpm g$^{-1}$)

r = mass accumulation rate (g cm$^{-2}$ yr$^{-1}$)

Table 2. $^{210}$Pb chronology of Puyuhuapi sediments. Σ inventories are the excess activity[a] accumulated beneath the surface.

| Core 35 | | | | Core 40 | | | |
|---|---|---|---|---|---|---|---|
| Depth (cm) | Σ Inventories (dpm cm$^{-2}$) | Age (yr) | time (yr AD) | Depth (cm) | Σ Inventories (dpm cm$^{-2}$) | Age (yr) | time (yr AD) |
| surface | 17.89 ± 0.06 | 0.0 | 2001 | surface | 12.43 ± 1.72 | 0.00 | 2001 |
| 1 | 17.28 ± 0.07 | 1.52 ± 0.04 | 1999 | 1 | 10.90 ± 1.57 | 4.21 ± 0.10 | 1997 |
| 2 | 16.60 ± 0.09 | 1.54 ± 0.07 | 1998 | 2 | 9.71 ± 1.43 | 3.75 ± 0.14 | 1993 |
| 3 | 15.88 ± 0.11 | 1.89 ± 0.06 | 1996 | 3 | 8.14 ± 1.27 | 5.67 ± 0.19 | 1987 |
| 4 | 14.83 ± 0.08 | 2.20 ± 0.05 | 1994 | 4 | 6.56 ± 1.09 | 6.98 ± 0.13 | 1980 |
| 5 | 13.72 ± 0.09 | 2.51 ± 0.04 | 1991 | 5 | 4.96 ± 0.91 | 9.03 ± 0.46 | 1971 |
| 6 | 12.63 ± 0.09 | 2.66 ± 0.03 | 1989 | 6 | 3.87 ± 0.77 | 8.02 ± 0.62 | 1963 |
| 7 | 11.58 ± 0.07 | 2.80 ± 0.03 | 1986 | 7 | 2.38 ± 0.58 | 15.62 ± 1.46 | 1947 ? |
| 8 | 10.63 ± 0.07 | 2.78 ± 0.03 | 1983 | 8 | 1.43 ± 0.40 | 16.45 ± 2.85 | 1931 ? |
| 9 | 9.80 ± 0.09 | 2.61 ± 0.08 | 1980 | 9 | 0.53 ± 0.20 | 32.05 ± 6.41 | 1899 ? |
| 10 | 8.98 ± 0.09 | 2.83 ± 0.04 | 1978 | | | | |
| 11 | 8.17 ± 0.03 | 3.03 ± 0.26 | 1975 | | | | |
| 12 | 7.36 ± 0.05 | 3.38 ± 0.16 | 1971 | | | | |
| 13 | 6.60 ± 0.05 | 3.50 ± 0.04 | 1968 | | | | |
| 14 | 5.89 ± 0.03 | 3.72 ± 0.12 | 1964 | | | | |
| 15 | 5.27 ± 0.06 | 3.59 ± 0.28 | 1960 | | | | |
| 16 | 4.67 ± 0.06 | 3.85 ± 0.07 | 1957 | | | | |
| 17 | 4.13 ± 0.04 | 3.97 ± 0.20 | 1953 | | | | |
| 18 | 3.65 ± 0.06 | 3.99 ± 0.32 | 1949 | | | | |
| 19 | 3.11 ± 0.06 | 5.22 ± 0.13 | 1943 | | | | |
| 20 | 2.68 ± 0.04 | 4.81 ± 0.22 | 1939 | | | | |
| 21 | 2.24 ± 0.04 | 5.69 ± 0.11 | 1933 | | | | |
| 22 | 1.86 ± 0.04 | 6.04 ± 0.18 | 1927 | | | | |
| 23 | 1.47 ± 0.04 | 7.53 ± 0.20 | 1919 | | | | |
| 24 | 1.10 ± 0.06 | 9.46 ± 1.36 | 1910 | | | | |
| 25 | 0.77 ± 0.06 | 11.34 ± 1.06 | 1899 | | | | |
| 26 | 0.46 ± 0.04 | 16.49 ± 0.21 | 1882 ? | | | | |
| 27 | 0.22 ± 0.04 | 23.82 ± 4.46 | 1858 ? | | | | |
| 28 | 0.06 ± 0.03 | 42.14 ± 9.46 | 1816 ? | | | | |

[a] $^{210}$Pb activity minus background obtained from the fixed exponential curve activity (1.62 ± 0.28; Core 40) and average values of the depth sections of the core (1.42 ± 0.04; Core 35)

? Data not included for estimation of accumulation rates of proxies

Table 3. Correlation of proxies between 1890-1980 and 1980-2001.

| | | Chlorins | THAA | Si-opal | MD | FWD | Rainfall anomaly |
|---|---|---|---|---|---|---|---|
| 1980-2001 | | | | | | | |
| | TOC | 0.50 | 0.46 | 0.32 | -0.20 | -0.63 | -0.68 |
| | Chlorins | - | **0.80** | 0.43 | -0.36 | **-0.77** | -0.61 |
| | THAA | - | - | 0.63 | 0.02 | -0.30 | -0.20 |
| | Si-opal | - | - | - | -0.30 | -0.12 | -0.15 |
| | MD | - | - | - | - | 0.68 | 0.25 |
| | FWD | - | - | - | - | - | **0.76** |
| | P. Index | - | - | - | - | - | 0.24 |
| 1890-1980 | | | | | | | |
| | TOC | **0.99** | **0.96** | **0.99** | **0.92** | **0.94** | -0.24 |
| | Chlorins | - | **0.92** | **0.99** | **0.94** | **0.91** | -0.21 |
| | THAA | - | - | **0.88** | **0.83** | **0.80** | 0.27 |
| | Si-opal | - | - | - | **0.96** | **0.93** | -0.40 |
| | MD | - | - | - | - | **0.99** | -0.52 |
| | FWD | - | - | - | - | - | -0.58 |
| | P. Index | - | - | - | - | - | 0.27 |

Values represent Pearson coefficients and bold numbers are significant correlations

($p < 0.05$)

TOC: Total organic carbon

THAA: Total hydrolyzable amino acids

MD: Marine diatoms

FWD: Fresh water diatoms

P. Index: Productivity Index

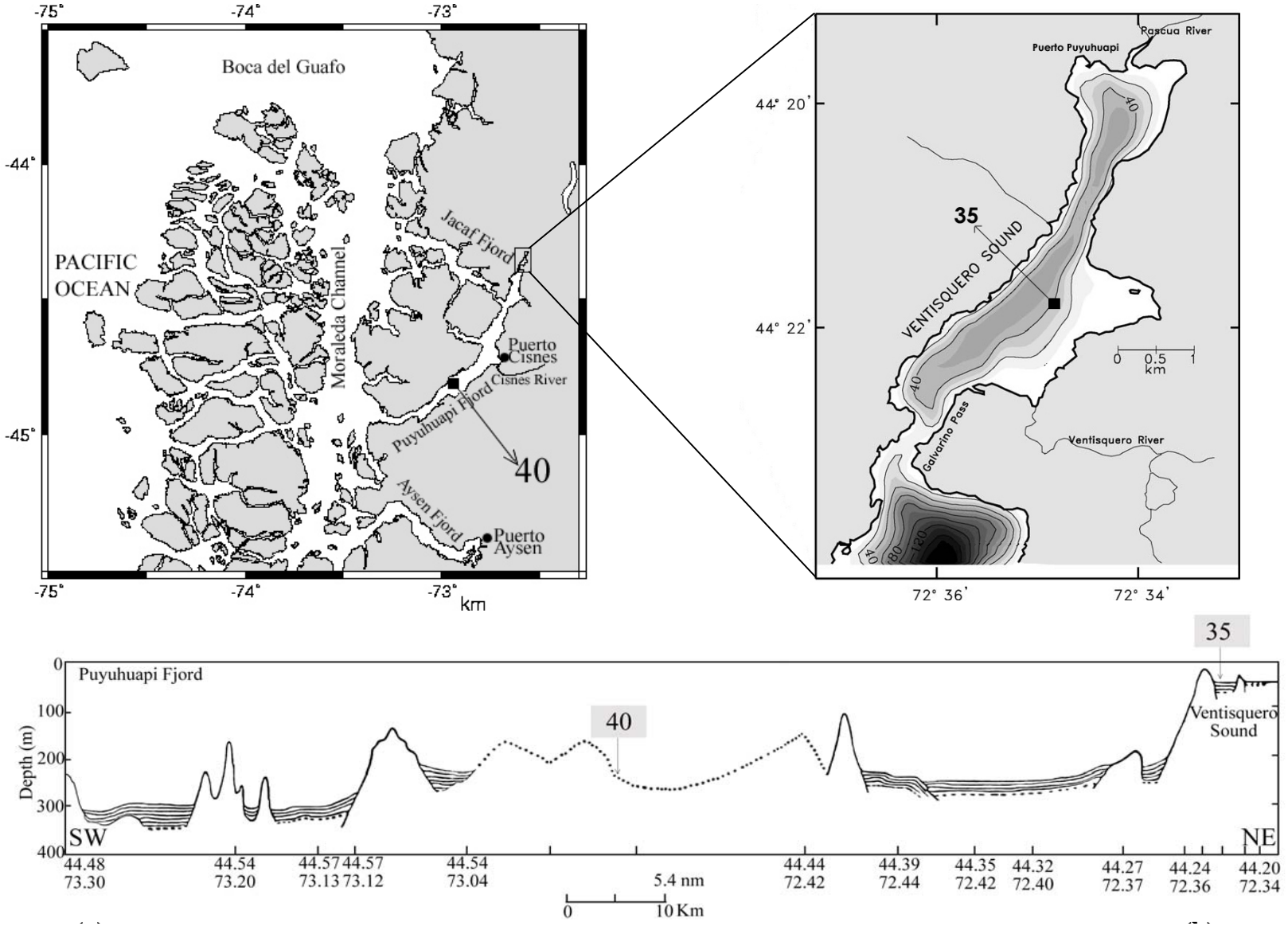


*Sepúlveda et al., Figure 1*

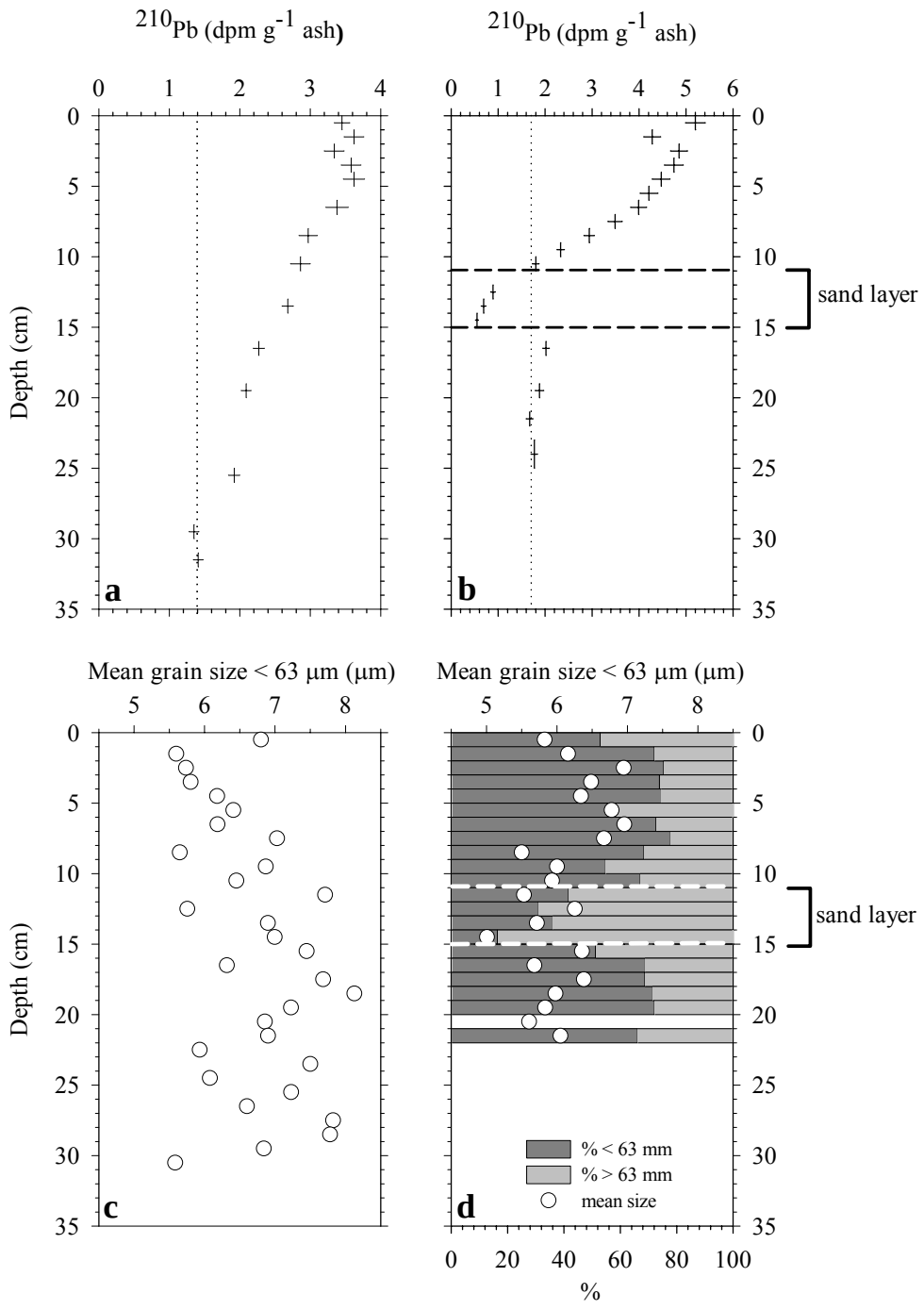


*Sepúlveda et al., Figure 2*

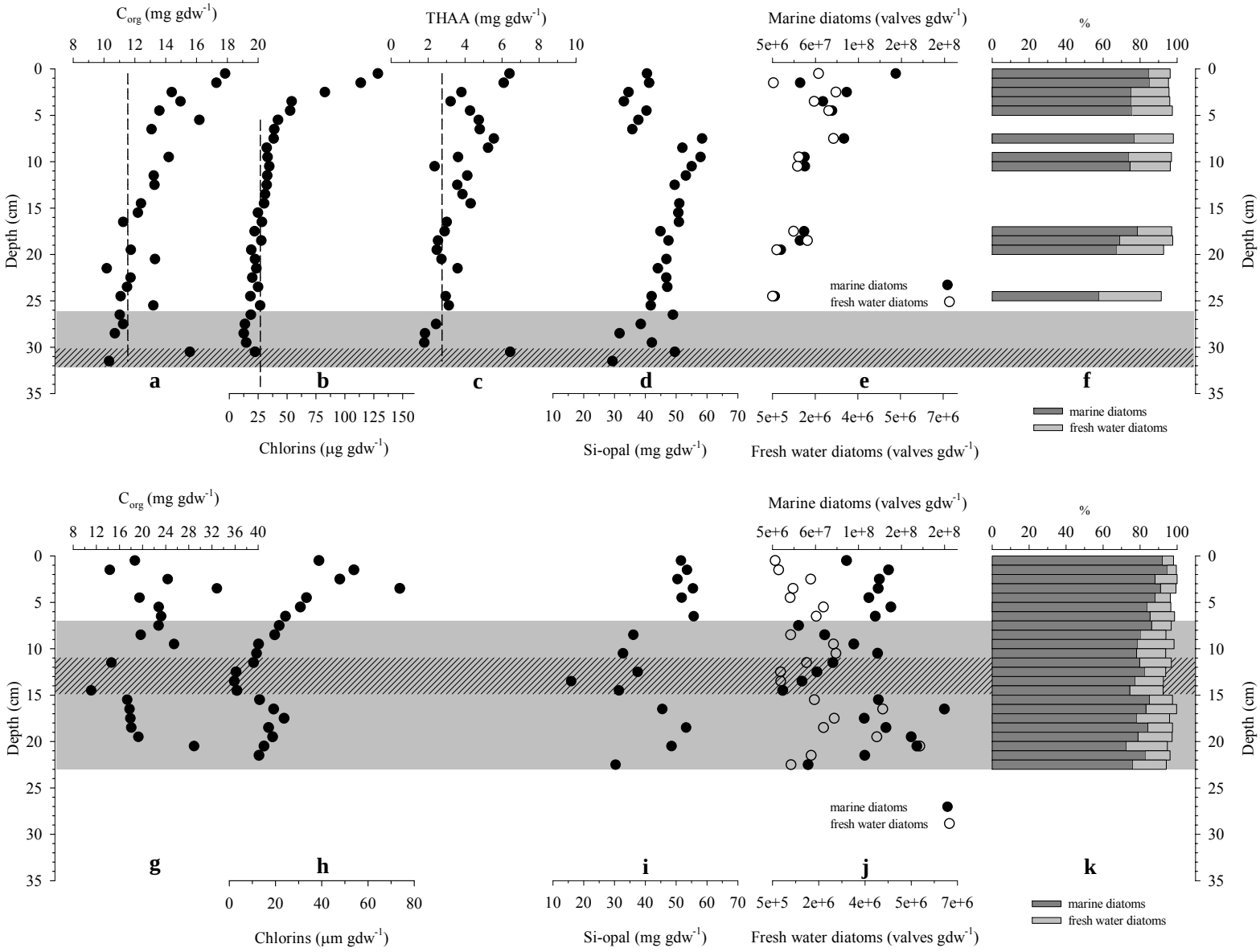


*Sepúlveda et al., Figure 3*

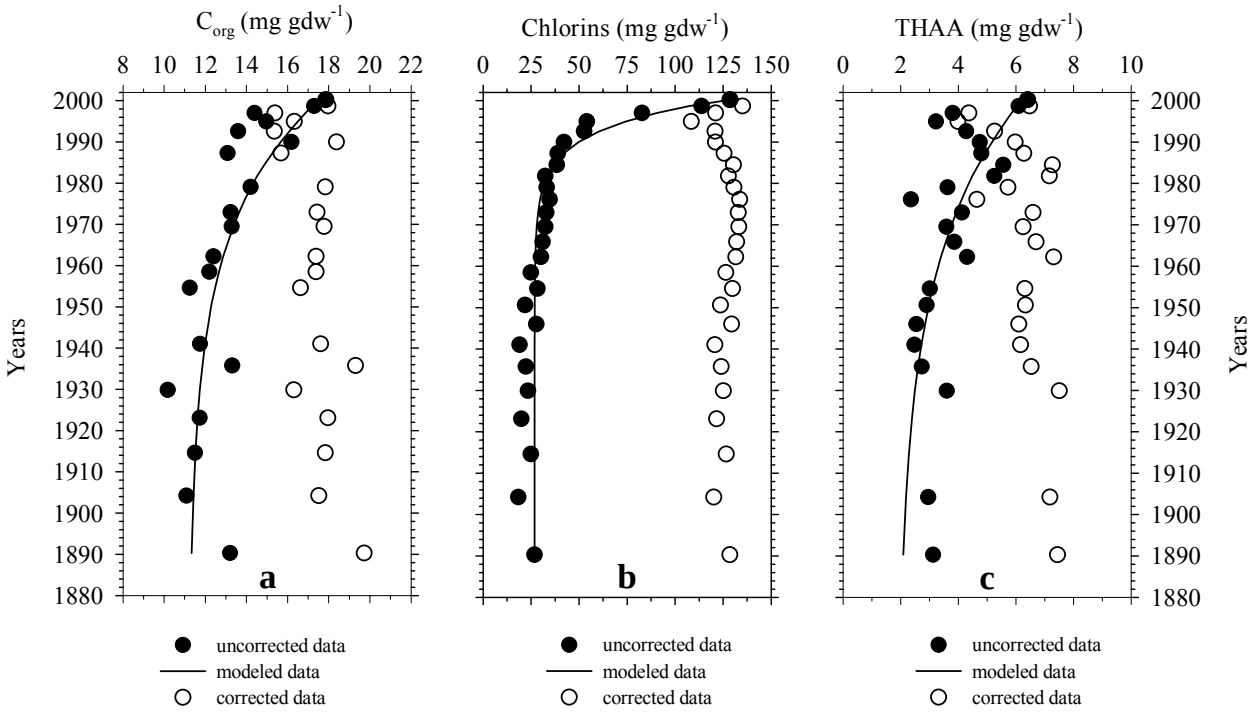


*Sepúlveda et al., Figure 4*

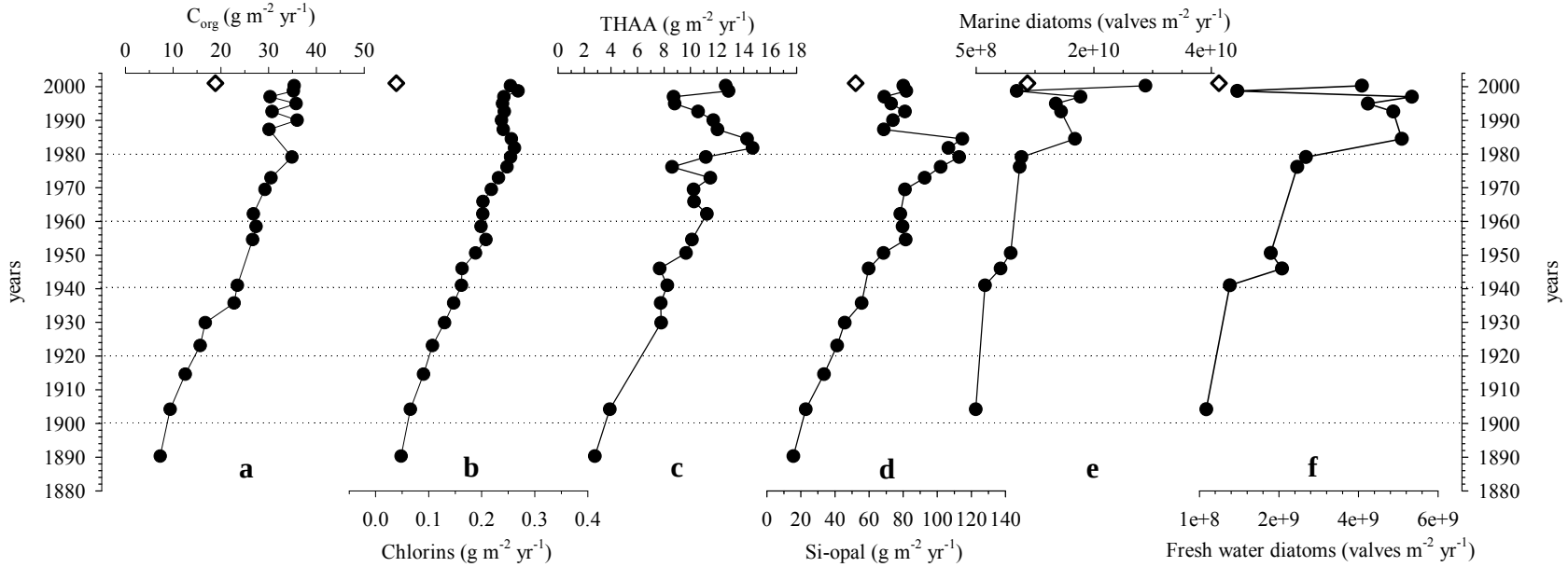


*Sepúlveda et al., Figure 5*

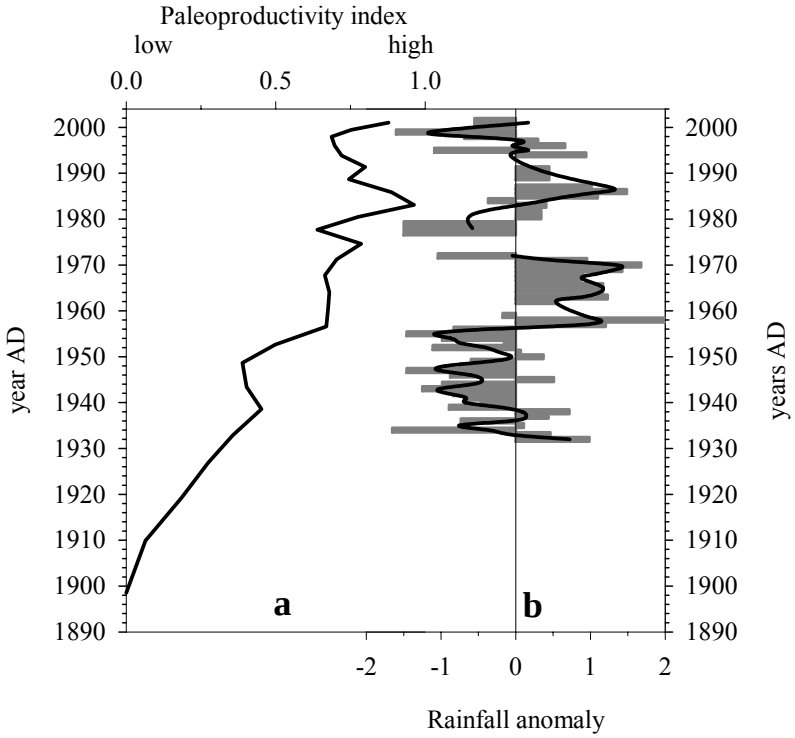


*Sepúlveda et al., Figure 6*